



Royal Netherlands
Meteorological Institute
*Ministry of Infrastructure and the
Environment*

Updating the calculation of ammonium particle formation in the Operational Priority Substances (OPS) source-receptor model

J. E. Williams, E. van der Swaluw,
F. Sauter, W. de Vries and A. van Pul

De Bilt, 2014 | Technical report; TR-350

Updating the calculation of ammonium particle formation in the Operational Priority Substances (OPS) source- receptor model

**Jason E. Williams, Eric van der Swaluw, Ferd
Sauter, Wilco de Vries and Addo van Pul**

KNMI Technical Report TR-350

Work performed in collaboration with the Air Quality Laboratory (LML), Public Institute of Health (RIVM).

Abstract

In this report we describe the methodology for calculating a new parameterization associated with ammonium particle formation in the Operational Priority Substances (OPS) model. For this purpose, a chemical box model was employed including using the latest reaction and photochemical data applied in the CB05 chemical mechanism, with particle formation being calculated with the ISOROPPIA II module. By deriving a dependence of the hourly conversion rate of gaseous NH_3 (K_{NH_3}) into NH_4^+ particles in %/hour on the concentration ratios of SO_2/NO_2 and NH_3/NO_2 over a range of atmospheric conditions, we have derived three different parameterizations representative of the night-time, morning/early evening and day-time conversion rates. We find that the rate of particle formation has strong diurnal cycle, as seen in observations, differing by an order of magnitude between the night-time and day-time due to an associated change in the main chemical precursors. When applying the various parameterizations in OPS we find that, although the introduction of a diurnal dependency in K_{NH_3} causes OPS to exhibit a significant low bias compared to the annually integrated measurements, adopting the new day-time K_{NH_3} parameterization results in an improvement of the performance of OPS when compared to multi-year surface measurements.

Contents

1. Introduction	(4)
2. Gaseous ammonia and Secondary Inorganic Aerosol in the troposphere	(6)
3. The formation of ammonium particles in the OPS Source-Receptor model	(8)
4. Methodology used for updating ammonium particle formation	(12)
4.1 Definition and sampling frequency of the meteorological stability classes	(12)
4.2 Description of the chemical box model	(13)
4.3 Meteorology adopted for the chemical simulations	(15)
4.4 Diurnal evolution of key trace gases and particulate species	(17)
5. The daily variability in ammonium particle formation (K_{NH_3})	(20)
5.1 Derivation of new ammonium particle formation rates	(21)
5.2 Sensitivity of K_{NH_3} towards meteorological parameters	(23)
5.3 Sensitivity of K_{NH_3} towards prescribed deposition velocities	(25)
5.4 Sensitivity of K_{NH_3} towards boundary layer height	(26)
6. Comparisons of particle formation rates	(27)
6.1 Temporal distribution of K_{NH_3} values for sample years	(27)
6.2 The application of the new K_{NH_3} values in OPS	(29)
7. Summary	(31)
8. References	(32)

1. Introduction

The Operational Priority Substances (OPS) model (van Jaarsveld et al. 2012) is used within the Public Health Institute of the Netherlands (RIVM) for the production of national concentration maps for particulate matter ($PM_{2.5}$, PM_{10}) across the Netherlands. These maps (GCN) show the temporal distribution and variability in the annual resident concentrations and total deposition estimates of PM. Secondary inorganic aerosols (SIAs) make up a large fraction of the total mass of both PM_{10} and $PM_{2.5}$ (van der Swaluw et al., 2013). This dominant fraction is commonly described as “secondary” i.e. not directly emitted such as primary PM (e.g. Black Carbon) but rather formed due to the oxidation of gaseous pre-cursors such as sulphur dioxide (SO_2), nitrogen oxides (NO_x) and ammonia (NH_3), which form sulphate (SO_4^{2-}), nitrate (NO_3^-) and ammonium (NH_4^+) particles, respectively. Their individual mass contributions towards the total measured SIA mass are $\sim 50\%$, $\sim 30\%$ and $\sim 20\%$, as shown in Figure 1 below.

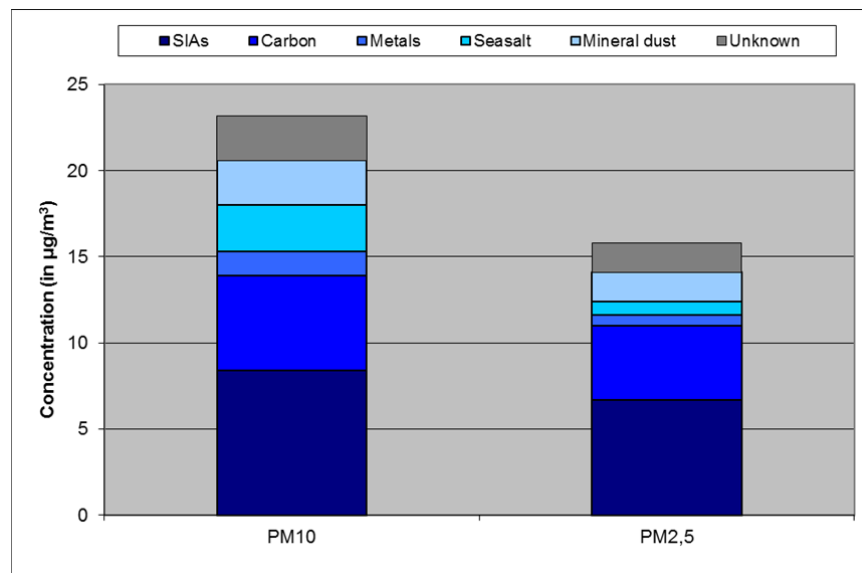


Figure 1: The different fractions of components that define the composition of PM_{10} and $PM_{2.5}$ in the Netherlands as derived from measurements (van der Swaluw, 2013).

The OPS model seriously underestimates the concentration of SIA when compared to the corresponding measurements, therefore bias-correction factors are used for the construction of GCN maps, such as that shown in Figure 2. Comparisons for recent years have shown that bias-correction factors of SIAs are currently 2.4 (SO_4^{2-}), 1.5 (NO_3^-) and 1.2 (NH_4^+) for the recent year of 2012 (Velders et al., 2013). In order to remove such model biases requires an assessment of the algorithms used for describing the rate and

efficiency of particle formation. This report focuses on parameterizing the formation of NH_4^+ particles from gaseous NH_3 into order to improve on the current simulations, which currently exhibit in a negative bias of $\sim 20\%$.

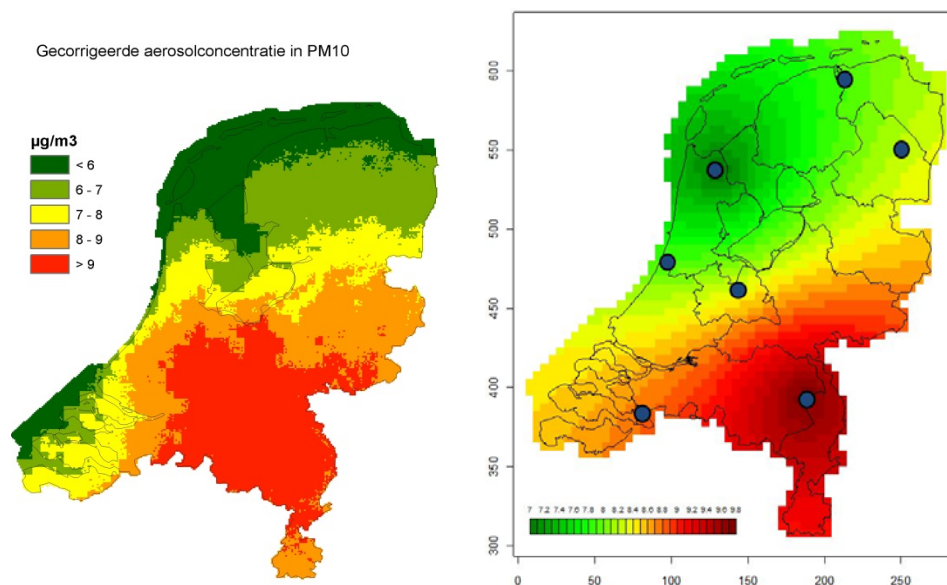


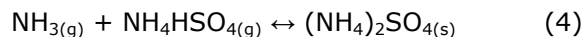
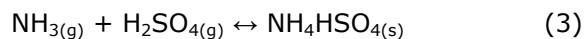
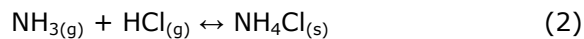
Figure 2: The calculated distribution of SIA concentrations from GCN over the Netherlands (left panel) for 2012 and an interpolation of measurements of SIA concentrations over the Netherlands for this same year (right panel). The dots in the right panel indicate the location of the seven monitoring stations that are used for performing the interpolation.

This technical report has the following structure: in Section 2 a concise overview is given regarding the sources and sinks of tropospheric NH_3 . Section 3 provides a description of the current parameterization that is used for calculating NH_4^+ particle formation in the OPS model. Section 4 presents a definition of the various meteorological classes (MSC) employed in the OPS, a definition of the chemical box-model used for determining the dependency of NH_4^+ formation on the gaseous precursors SO_2 , NO_x and NH_3 and a description of how the various MSC classes are used in the new derivation. We also provide some examples of how selected gas phase precursors and SIA change with respect to time. Section 5 focuses on the derivation of the new NH_4^+ particle formation rates and the relationship between day-time and night-time values. We also examine the sensitivity of the resulting K_{NH_3} parameterization towards the meteorological variability employed, deposition rates and the prescribed boundary layer height. Section 6 shows a comparison of the temporal distribution of K_{NH_3} values over the Netherlands. Finally, section 7 gives a summary and recommendations for the use of the new ammonium module in the OPS-model.

2. Gaseous ammonia and Secondary Inorganic Aerosols formation in the troposphere

Ammonia (NH₃) emissions occur throughout the Northern Hemisphere, where they predominantly originate from agricultural practises (Bouwman et al., 1997; Pinder et al, 2004; Sutton et al, 2011). The strength of the emission fluxes exhibit a strong temperature dependence (Skjøth and Geels, 2013), meaning they exhibit a high seasonal and daily variability (Geels et al, 2012). Once emitted, the direct oxidation in the gas phase by OH (forming the NH₂ radical) is relatively slow, meaning the atmospheric lifetime is principally determined by the cumulative loss from the rate of condensation into SIA, scavenging and dissolution into liquid droplets and/or deposition onto the surface (Seinfeld and Pandis, 2006). Although peak mixing ratios occur near strong source regions, gaseous NH₃ rapidly transforms into SIA, equating to ~5% per hour in North-West Europe (van Jaarsveld et al., 2012). Measurements have shown that particle number concentrations are to be critically dependent on meteorological parameters such as wind direction and boundary layer height (Väkevä et al, 2000).

There are four main forms of ammonium particles present in the troposphere, these being ammonium nitrate (NH₄NO₃), ammonium chloride (NH₄Cl), ammonium bisulphate (NH₄HSO₄) and ammonium sulphate ((NH₄)₂SO₄), as described below in Eqns 1-4:



Depending on the Relative Humidity (RH), particles may exist in either a solid or a hydrated form due to the hygroscopic nature of the compounds, although the RH is usually sufficiently high such that ammonium particles exist as aquated salt solutions (i.e.) the compounds dissociate into ionic form (e.g. ammonium (NH₄⁺), sulphate (SO₄²⁻)). Thermodynamic considerations mean that, once formed, NH₄HSO₄ and (NH₄)₂SO₄ are relatively stable, and are the preferred state for NH₄⁺, whereas NH₄NO₃ and NH₄Cl exist in equilibrium and therefore may dissociate at higher temperatures back into the gaseous precursors NH₃ and Nitric Acid (HNO₃)/Hydrochloric Acid (HCl). Although HCl exhibits low resident mixing ratios over land due to enhanced washout, it can be released from sea-salt particles (NaCl) making this form of ammonium particle most relevant along coasts. The chemical environment under which such particles form determines the frequency of occurrence of each particle type. For countries like the Netherlands, where lower tropospheric composition is high in nitrogen oxides (NO_x) and

NH₃, but low in sulphur dioxide (SO₂), NH₄NO₃ comprises the dominant fraction of the SIA. A further complication is the behaviour of multi-component aqueous systems. For more information, the reader is referred to the comprehensive treatise given in Seinfeld and Pandis (2006).

The efficient formation, and subsequent deposition, of SIA has consequences ranging from increases in radiative forcing of the lower atmosphere (Xu and Penner, 2012), acidification and eutrophication of natural ecosystems (e.g. Stevens et al, 2010) and reduced visibility (Tang et al., 1967). Direct health effects are highly uncertain (Sutton et al., 2011), although indirect effects such as the dampening of tropospheric ozone (O₃) formation by both additional scattering and NO_x sequestration could be considered to be beneficial.

3. The formation of ammonium particles in the OPS model

The formation rate of NH_4NO_3 and $\text{NH}_4\text{HSO}_4/(\text{NH}_4)_2\text{SO}_4$ particles is critically dependent on the resident mixing ratios of HNO_3 and NH_3 . The equilibrium state between gaseous precursors and particles is determined by accounting for the resident concentrations of SO_4^{2-} , NO_3^- and NH_4^+ , where the influence of both temperature and RH are accounted for with respect to determining the rate of particle growth. In the current OPS model the rate of formation of ammonium SIA is parameterized using a 1-D column model, which accounts for the chemical evolution of the pre-cursor gases and deposition processes (de Leeuw et al., 1990). By prescribing resident concentrations of SO_2 , NO_x , NH_3 , O_3 and OH , and using measured meteorological data, the conversion rate of NH_3 into NH_4^+ (in %/hr) has been derived with respect to both $[\text{NO}_2]/[\text{NH}_3]$ (C_1 in ppb/ppb) and $[\text{SO}_2]/[\text{NH}_3]$ (C_2 in ppb/ppb), as described in equation (5). No distinction is made regarding the different rates of particle formation during day and night. When applied in OPS a check has to be made that negative K_{NH_3} values do not occur by adopting a lower limit of 1% for K_{NH_3} and an upper limit for C_2 of ~ 3 .

$$k_{\text{NH}_3} = \max(1.0, 0.8 + 2.4 C_1 + 18.9 C_2 + 5.4 (C_2)^4 - 0.51 (C_2)^6) \quad (5)$$

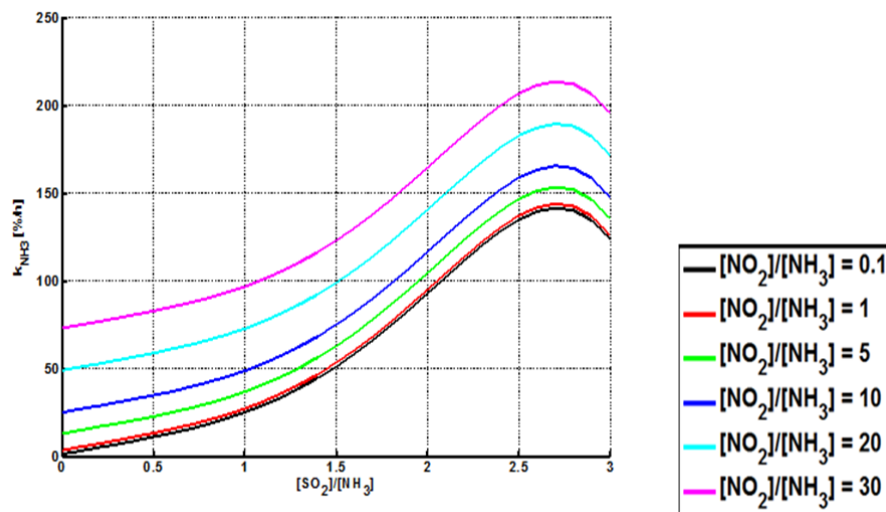


Figure 3: The dependence of K_{NH_3} (in %/hr) on C_2 as implemented in the OPS model. A conversion rate of 200% should be interpreted as 100% conversion within 30 minutes. Different K_{NH_3} values are shown for a range of C_1 values covering the range found in the Netherlands.

Figure 3 shows the resulting variability in K_{NH_3} with respect to the C_2 ratio for a number of chosen C_1 ratios relevant for the Netherlands. The resulting dependencies exhibit a shallow sigmoidal shape, with maximum values of $> 150\% \text{ hr}^{-1}$ NH_3 conversion for C_2 ratios > 2.0 i.e. under relatively high SO_2 concentrations. For the present day, the C_2 ratio rarely exceeds 1.0, except around the coastline, which has relatively low NH_3 concentrations. Average conversion rates for conditions typically found in the Netherlands equate to $\sim 16\%/hr$ in 1980 falling to $\sim 5\%/hr$ in 1997 (van Jaarsveld et al., 2012).

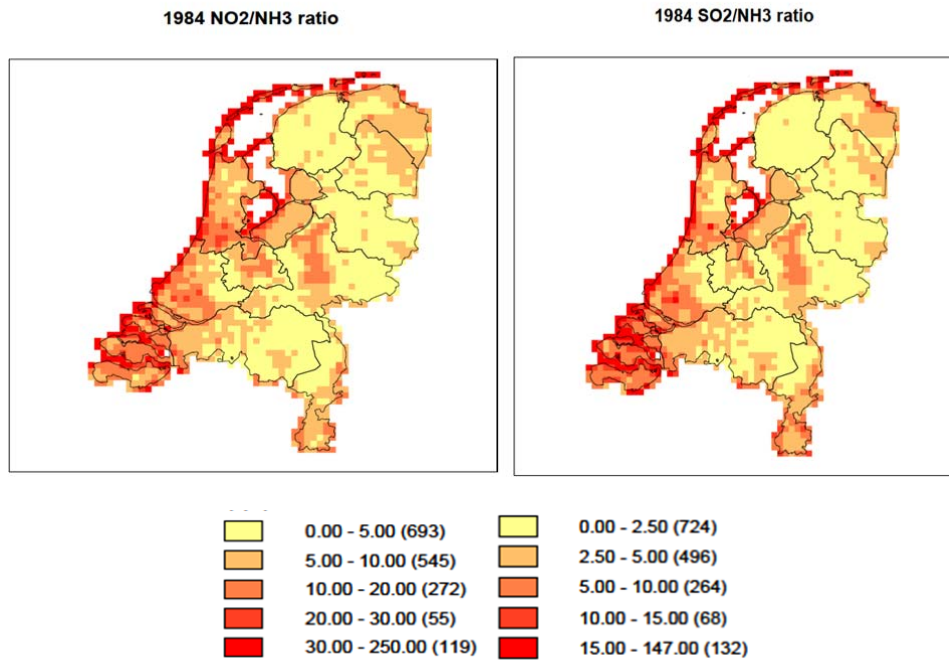


Figure 4: The ratio of (left) NO_2/NH_3 and (right) SO_2/NH_3 for the year 1984 as used in the OPS model on a $5 \times 5\text{km}$ horizontal grid.

Figures 4 and 5 show the range and temporal distribution of C_1 and C_2 ratios used in the OPS model for calculating K_{NH_3} for the years 1984 and 2005, respectively, with the corresponding scales for each map being directly underneath each panel. Also shown are the total numbers of incidences for each ratio range. These ratio maps are produced using background concentration maps for the concentration of the precursor species, which are fixed for the entire year (i.e.) the ratios do not change with respect to season. There is a high temporal variability in both of the ratios, with the highest values being found towards the west over the Zeeland region and the lowest in the North around Friesland. This is due in part to lower regional emissions of NH_3 at the coast and the enhanced loss of NH_3 over the sea.

The strong mitigation practices applied for NO_x and SO_2 emissions over the last twenty years have resulted in a significant reduction in the range of both ratios. This results in the max ratio band for C_1 and C_2 falling by approximately an order of magnitude, from 30-250 to 30-40 and from 15-147 to 10-11, respectively. Moreover, the incidence of events in the highest bin also falls by approximately an order of magnitude. Future projections in the changes in regional emissions for the Netherlands project little change

for NH_3 , coupled with a continual decline in NO_x emissions (Velders et al., 2013). Thus, it is expected that the C_1 ratio exhibits further decreases in future years (see below).

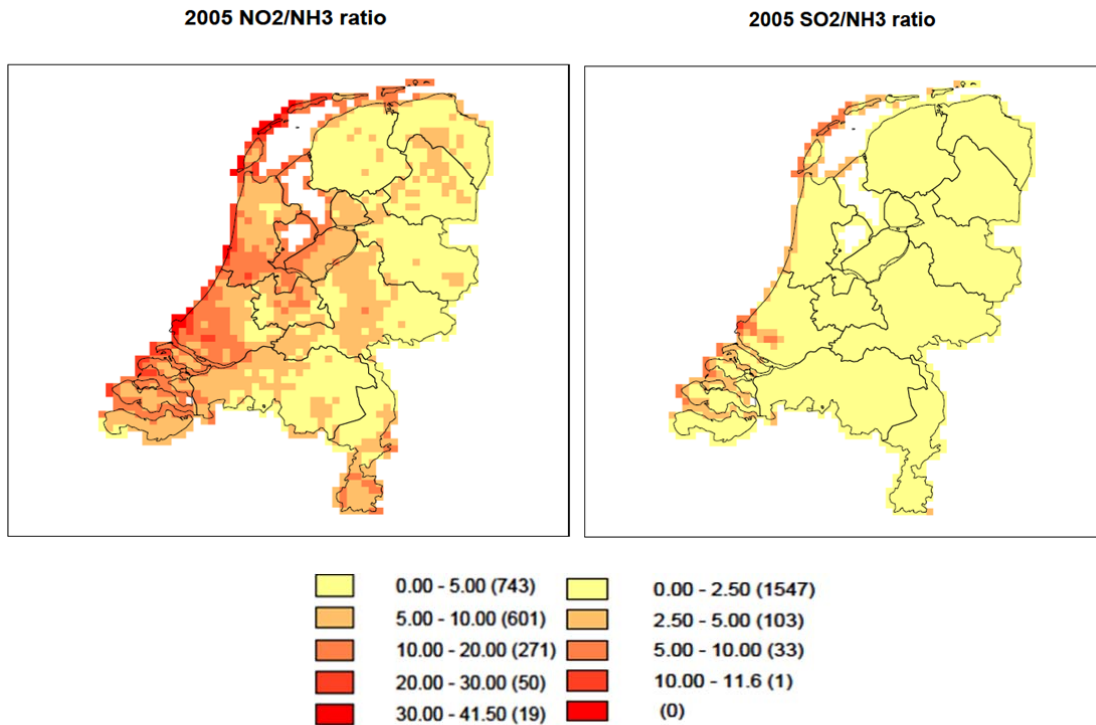


Figure 5: As for Figure 4 except for 2005.

The frequency distribution of both C_1 and C_2 ratios relevant for the Netherlands has also changed over the last 30 years as shown in Figure 6. To highlight this we also show the variation in both ratios that occur for the 25th, 50th and 75th percentile across the timeline 1984-2015. Although the C_2 ratio has fallen significantly over the past decades, it has been relatively constant since 2000. In contrast, the change in the C_1 ratio follows a rather different pattern, where the increase in NO_x emissions from increasing Road Traffic results in a rather saw-tooth decrease in C_1 between the 1990's and 2000's.

In Figure 7 we show the correlation between the C_1 and C_2 ratios as shown in Figs. 5 and 6, expanded for the four years for which background maps are available. For both years shown the majority of points lie in the range of $C_1=0-20$ and $C_2=0-5$. It can be seen that C_1 and C_2 are highly correlated meaning that the spread of the points lies within a more constrained range of values than is theoretically possible. For instance, the combination of high C_1 and low C_2 does not occur, same for low C_1 and high C_2 . This means regions with high SO_2 emissions also exhibit high NO_x emissions, usually under scenarios with low NH_3 mixing ratios thus resulting in high ratio values. Conversely, the high background NH_3 values limit the range of both C_1 and C_2 .

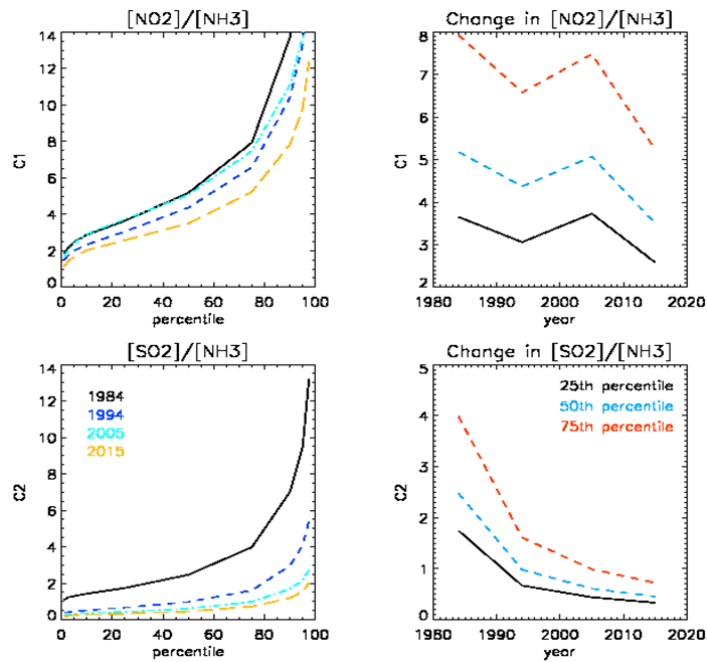


Figure 6: The change in distribution of C_1 (top) and C_2 (bottom) values across the timeline 1984-2015. Also shown is the change in both values at the 25th, 50th and 75th percentile with respect to year.

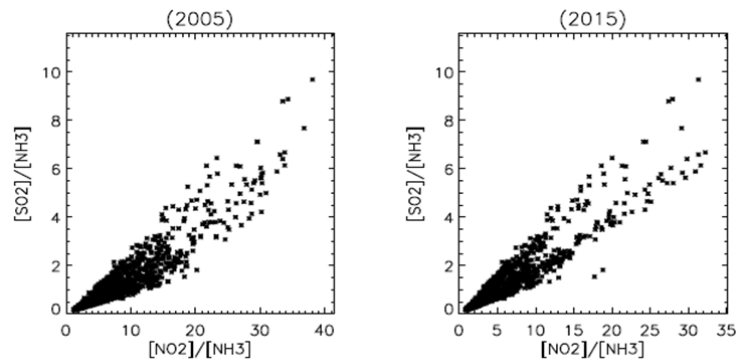


Figure 7: The correlation between ratios C_1 and C_2 in the background maps used for calculating the K_{NH_3} conversion rate. The reader should note the different scales used for plotting

4. Methodology for updating the formation rate of NH₄ particles.

4.1 Definition and sampling frequency of Meteorological Stability Classes

When calculating the transport and deposition of atmospheric particles the OPS model indexes a set of predefined meteorological stability classes (MSC) during the simulation of particle formation. There are six types of MSC namely, U1, U2 (Unstable), N1, N2 (Neutral) and S1, S2 (Stable). Table 1 below shows some associated meteorological parameters associated with each MSC based on statistical evaluations of data provided by KNMI over the decade 1990-1999.

Meteorological Parameter		Unit	U1	U2	N1	N2	S1	S2	Avg*
Frequency of Occurrence		%	10	22	18	17	13	20	
Wind speed at 10m	u_{10}	m s ⁻¹	2.5	3.9	3.9	6.9	1.3	2.6	2.9
Wind turning 10-200m	A	degrees	8	0	11	3	27	20	10
Temperature	T	°C	11	16	9	8	7	8	10
Global radiation	Q_g	W m ⁻²	206	378	20	22	2	3	114
Precipitation probability	P_p		0.04 1	0.037	0.105	0.202	0.019	0.045	0.077
Precipitation intensity	R_i	mm hr ⁻¹	1.26	1.53	1.15	1.10	1.06	1.24	1.22
Length of prec. events	\hat{Q}_w	hr ⁻¹	1.7	1.5	2.0	2.5	1.7	1.8	2.0
Relative humidity	RH	%	83	67	88	86	92	89	83
Space heating Coefficient	stC	°C	6.6	5.4	10.0	16.2	5.7	8.0	8.7
Sensible heat flux	H_0	W m ⁻²	36	80	-25	-39	-3	-19	6
Friction velocity	u^*	m s ⁻¹	0.28	0.43	0.36	0.68	0.53	0.18	0.19
Monin Obukhov length	L	m	-47	-64	196	701	6	32	44
Mixing height	$z_{l,max}$	m	231	888	290	540	42	146	165
Aerodynamic resistance	$R_a(4)$	s m ⁻¹	22	15	21	11	240	46	24
Aerodynamic resistance	$R_a(50)$	s m ⁻¹	34	24	45	21	862	133	47

Table 1: Meteorological parameters associated with the six different MSC employed on the OPS model. Values used are averages of Meteorological data for the Netherlands between 1990 and 1999 provided by KNMI.

These associated meteorological variables place constraints on the values chosen during the calculation of new particle formation rates. The variation in temperature, global radiation and boundary layer height in Table 1 shows that the U1/U2 MSC is associated with the day-time boundary layer, whereas the S1/S2 MSC is associated with the night-

time boundary layer. The N1/N2 MSC are representative of conditions that can occur throughout the day, where the global radiation value indicates an overcast day will low intensity irradiance. Figure 8 shows the sampling frequency of each MSC with respect to the time of day as integrated across the years 1994-2005. In agreement with Table 1 it shows that the S1/S2 are mostly sampled during the night and the U1/U2 during the day, with the N1/N2 MSC exhibiting a rather homogenous distribution. This allows the use of two different particle formation rates in OPS by indexing with respect to the U and S MSC, relevant for day-time and night-time conditions.

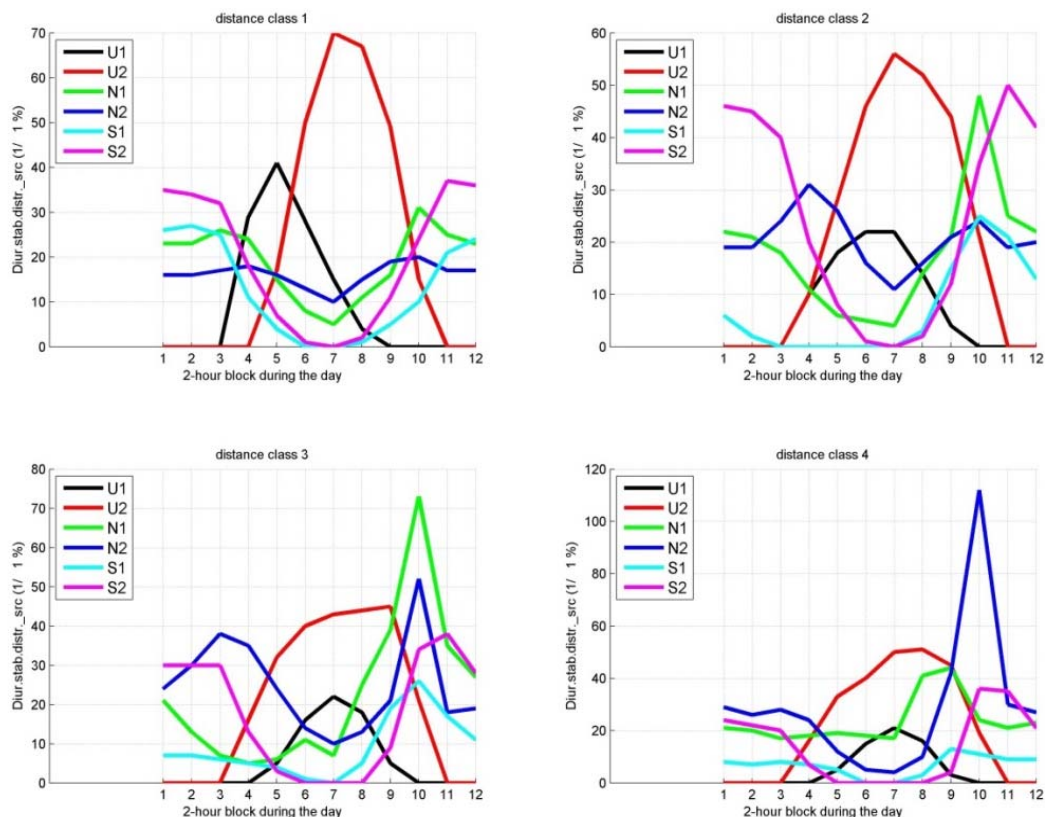


Figure 8: The sampling frequency of the six different MSC integrated for the years 1994-2005 for four different distance classes. Distance classes 1 and 2 are most relevant to the emissions that originate from the Netherlands.

4.2 Description of the Chemical Box model

The chemical box model employed is a modified version of that used for investigating the impact of chemical processes and updates to reaction data on the composition of the troposphere (Williams and van Noije, 2008). For this exercise, the box model uses the CB05 chemical mechanism (Yarwood et al, 2005) for the description of chemical processes, as currently used in a number of different regional Chemistry-Transport Models (CTMs) for performing air quality studies. We supplement CB05 with gas phase reactions of both SO₂ and NH₃, thus allowing for the formation of SIA components. In order to account for the fast oxidation of SO₂ into SO₄⁻ in cloud droplets, we include a

first-order conversion rate similar to that now included in the OPS model for the improvement of SO_4^- distributions (van der Swaluw et al., 2013). The differential chemical equations are solved using the TWOSTEP solver (Verwer, 1994), which uses an iterative approach using a variable chemical time step.

The CB05 chemical mechanism has been updated using reaction rate and photochemical absorption data taken from the latest recommendations (e.g. Sander et al, 2011). The photolysis rates are calculated using the tropospheric version of the modified band approach (Williams et al, 2006) using the Practical Improved Flux Method (PIFM) 2-stream radiative transfer solver (Zdunkowski et al., 1980). The resulting photolysis frequencies are derived by integrating across the wavelength range 202-650nm. The impact of using this approach on tropospheric composition has been recently examined in the global 3D CTM TM5 (Williams et al, 2012). The actinic flux (i.e. the spherically integrated flux of photons at any point in the atmosphere) is constrained by applying pre-defined atmospheric profiles for ozone (O_3), temperature and pressure. Additional scattering and absorption of light by clouds and aerosols is accounted for using the parameterization of Slingo (1989) and the aerosol climatology of Shettle and Fenn (1979), respectively. Partial cloud coverage is accounted for using the approach of Geleyn and Hollingsworth (1979).

For particle formation the ISORROPIA II thermodynamic equilibrium model (Fountoukis and Nenes, 2007) has been introduced, which calculates the resident concentrations of SO_4^- , NO_3^- and NH_4^+ depending on RH, temperature and the pre-cursor gas concentrations of NH_3 and HNO_3 and existing particle concentrations. Although ISORROPIA II also has the ability to calculate NH_4Cl concentrations, we neglect their influence in this study. Modelling of previous field studies related to simulating NH_4NO_3 particle formation in the convective boundary layer at Cabauw has shown that ISORROPIA II has difficulty in partitioning the correct gas and aerosol phase fractions due to an enhanced rate of particle formation (aan de Brugh et al. 2012). However, we use ISORROPIA II without any scaling applied, as this empirical factor may change with respect to tropospheric conditions. The variability in the Aerosol Optical Depth (AOD) parameter used for calculating the photolysis rates is not coupled to the output from ISORROPIA II and, thus, the subsequent increase in particle number density with respect to time is not accounted for.

Initial conditions of key gaseous species such as tropospheric O_3 , NH_3 , HNO_3 and NO_x are based on values that are representative of mixing ratios in the first 500m of the boundary layer over the Netherlands i.e. relatively high mixing ratios NH_3 and NO_x and low mixing ratios of SO_2 . As the simulation starts at 0:00 UT, we partition the NO_x at 10% NO and 90% NO_2 , where photolytic regeneration of NO does not occur for the first 5 hours of the simulation due to lack of light. The initial SO_4^- , NH_4^+ and NO_3^- particle concentrations are set to values which are representative of the background concentrations as derived from measurement stations in the Netherlands. The initial conditions for the other species such as isoprene were taken from a TM5 simulation conducted for the present day using AR5 anthropogenic emission estimates (Lamarque et al, 2010), GFEDv3 biomass burning emissions (van der Werf et al, 2010) and MEGANv2.1 biogenic emissions (Guenther et al., 2012).

The emission and deposition fluxes were altered such that the diurnal evolution of the most important trace gases and particles remained realistic throughout the simulation period. The emission of isoprene has a diurnal profile imposed, where maximal emissions

occur at 12 UT to account for diurnal variations in biogenic activity. The NH₃ emissions have a temperature dependency applied, where there is less emission during night-time than day-time as defined by the daily evolution in the temperature profile (c.f Figure 10)

Species	Vd (m ² s ⁻¹)	Species	Vd (m ² s ⁻¹)	Species	Vd (m ² s ⁻¹)
NO	0.09	SO ₂	1.0	CH ₃ COOH	0.35
NO ₂	0.09	SO ₄	0.85	CH ₃ CH ₂ OH	0.2
NO ₃	0.05	HCHO	0.8	ALDX	0.15
HNO ₄	0.09	CH ₃ OOH	0.15	PANX	0.1
HNO ₃	1.0	PAN	0.3	ISPD	0.15
N ₂ O ₅	0.045	CH ₃ COCHO	0.3	NH ₃	1.0
H ₂ O ₂	1.2	RONO ₂	0.8	HONO	0.2
CO	0.05	ROOH	0.25	NO3_a	1.0
O ₃	0.2	ALD2	0.25	NH4_a	0.5
CH ₃ OH	0.5	HCOOH	0.9		

Table 2: Deposition velocities applied in the chemical box model given in m² s⁻¹.

To prevent the excessive titration of O₃ we scaled down the NO_x emissions during the night and gradually increase them during the morning in order to be more representative of daily variations due to road traffic, which acts a dominant source of NO_x emissions in the Netherlands. Due to the lack of wet deposition and venting of the boundary layer in the box model, the deposition velocities implicitly include an additional term for such processes, especially loss of particles by growth and gravitational settling with no size spectrum imposed on the particles. The deposition velocities employed in the simulations are given above in Table. 2.

4.3 Meteorology adopted for the chemical simulations

Although there will be a temperature driven seasonal dependency in both biogenic emission fluxes of e.g. Isoprene, NO and Non Methane Hydro-Carbons (NMHC) and the efficiency of particle formation, we select conditions which can be considered to be representative of the annual mean. Therefore, we chose a simulation date of the 31st March, which provides an approximate mean for the number of daylight hours (and thus

the extent of photochemical processing) and use the US standard atmosphere (NOAA, 1976) for defining vertical properties of the atmospheric column above the box.

A fixed simulation time of two days is chosen for the simulations. The first day was used as a spin-up period to allow the system to reach chemical equilibrium from the initial starting conditions. The conversion values are sampled on the second day of each simulation. To avoid an artificial upper limit for K_{NH_3} , we use a chemical time step of 10 minutes to solve the differential equations. We subsequently scale up this conversion rate to K_{NH_3} ($\% \text{hr}^{-1}$), meaning that conversion rates can exceed 100% as shown for the old parameterization (see Fig. 3). We output the hourly values of percentage NH_3 conversion, along with the associated C_1 and C_2 ratios plus the solar zenith angle, which are used for partitioning the values between day and night. Although the first day of simulation is skipped to allow chemical equilibrium to be achieved, the night-time values are sampled between 1am-6am ($\text{sza} > 85^\circ$ and $< 115^\circ$). The morning/evening values between 8am-10am/5pm-6pm ($\text{sza} > 66^\circ$ and $< 55^\circ$) and the day-time sampled between 10am-3pm ($\text{sza} < 55^\circ$). This avoids using values at the beginning and end of the day when the change in photochemical activity can cause spurious values.

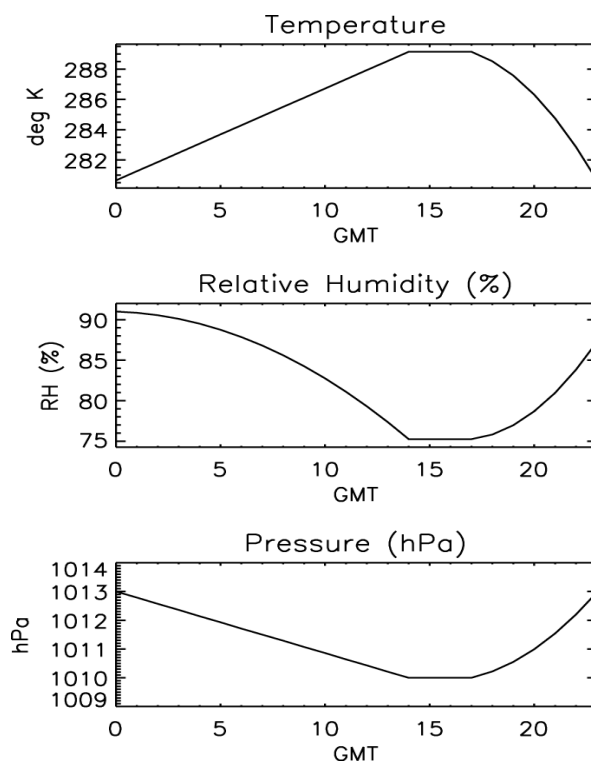


Figure 9: The diurnal evolution in temperature (top), relative humidity (middle) and pressure (bottom).

Figure 9 shows the diurnal variability imposed on the meteorological variables. Based on the average values provided for the MSC in Table 1, the temperature profile during the day varies from 7.5°C-13°C, with the maximum temperature occurring at 14:00 UT. A corresponding decrease in pressure is also imposed resulting in a reduction in the surface pressure by a few hPa. A similar approach to the RH is also applied, where night-time values are RH=91% falling during the day to 75%, based on the averages from the relevant MSC. Although this represents a relatively large variation across any day we

choose this as directed from the values used in the OPS model. For reasons of numerical stability, we fix the boundary layer height at 500m throughout the day, which is somewhat lower than the height prescribed in other studies (e.g. Ervens et al., 2003).

4.4 Diurnal evolution of key trace gases and particulate species

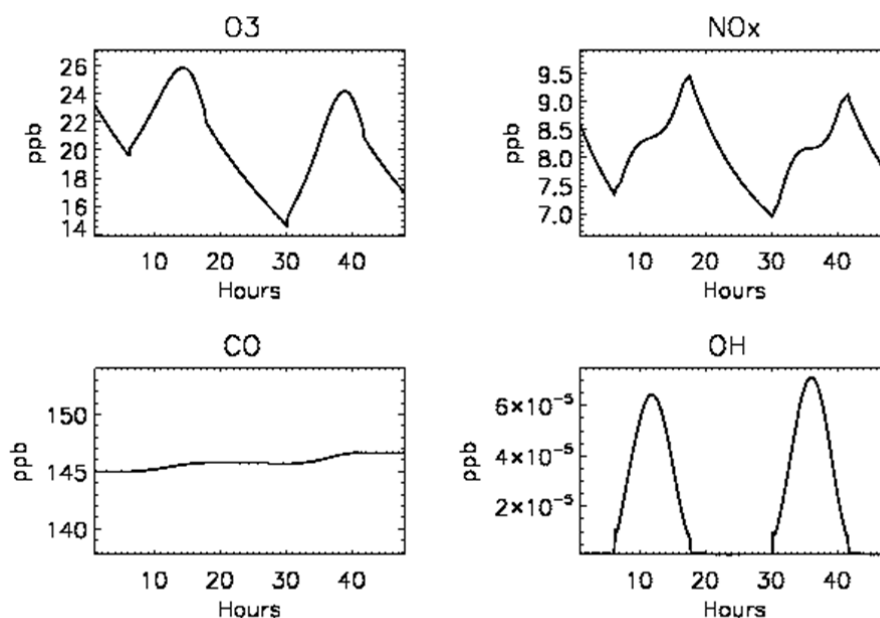


Figure 10: The daily evolution of O_3 , NO_x , CO and OH mixing ratios for a simulation adopting initial conditions of 25ppb ($49 \mu\text{g}/\text{m}^3$) O_3 , 6ppb ($4.2 \mu\text{g}/\text{m}^3$) NH_3 , 8ppb ($9.8 \mu\text{g}/\text{m}^3$) NO_x and 3ppb ($7.9 \mu\text{g}/\text{m}^3$) SO_2 .

Figures 4 and 5 provide a range of C_1 and C_2 ratios as taken from the OPS model for a historical and present day scenario. We subsequently use this as a guide towards what ratios need to be covered during the box model simulations in order to cover the necessary parameter space needed for running the OPS model. For this to be realised, ~ 150 box model simulations were performed using different initial conditions and $NO_x/NH_3/SO_2$ emission fluxes. The range used for the initial conditions was 25-38 ppb ($49-75 \mu\text{g}/\text{m}^3$) O_3 , 0.2-10 ppb ($0.5-26 \mu\text{g}/\text{m}^3$) SO_2 , 1-15 ppb ($0.7-10.4 \mu\text{g}/\text{m}^3$) NH_3 and 5-9 ppb ($6.1-11 \mu\text{g}/\text{m}^3$) NO_x , chosen to be representative of the Netherlands. In the box model, 90% of the NO_x emissions are introduced as NO , thus rapid titration of O_3 occurs immediately after each simulation is started. Therefore, as the initial NO_x mixing ratios are increased, the initial O_3 mixing ratios are also increased to prevent unrealistically low O_3 mixing ratios after a few hours of each simulation. Box model simulations typically use NO_x mixing ratios of the order of a few ppb (e.g. Ervens et al, 2003) whereas for our simulations we use conditions relevant to the polluted Netherlands. Therefore, we vary the NO_x emissions through the day as described in Sect. 4.2.

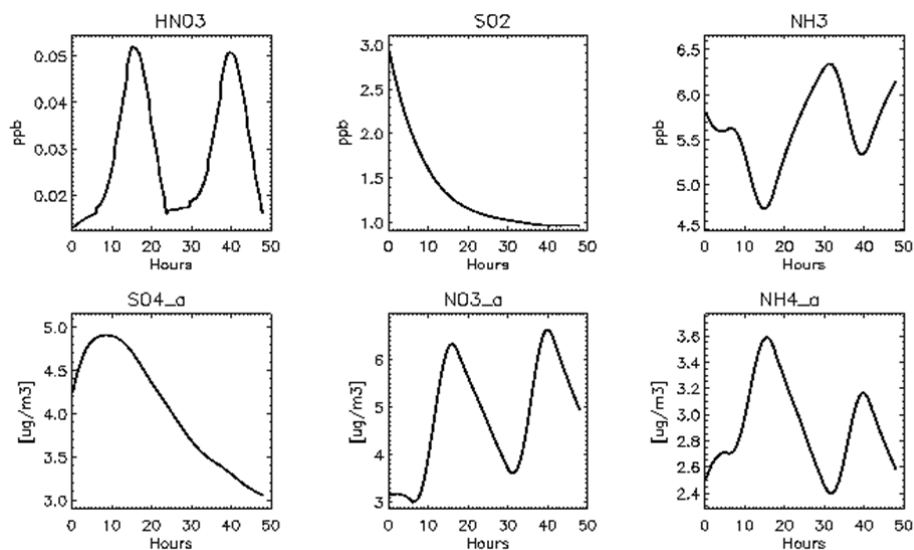


Figure 11: The daily evolution HNO_3 , SO_2 and NH_3 , along with the changes in the particle concentrations for SO_4^{2-} , NO_3^- and NH_4^+ given in $\mu\text{g}/\text{m}^3$

Figure 10 shows an example of the evolution of O_3 , NO_x , CO and OH throughout a two-day simulation period with moderate initial SO_2 mixing ratios, with further details related to the initial conditions being provided in the figure caption. Figure 11 shows the corresponding evolution in HNO_3 , SO_2 and NH_3 , along with the resulting particle concentrations for SO_4^{2-} , NO_3^- and NH_4^+ . This simulation represents an air parcel that originates in a relatively polluted urban scenario such as around Rotterdam port and then travels across the Netherlands in a North Easterly direction whilst becoming photochemically aged.

In the first hours of the simulation, the gaseous SO_2 is rapidly converted to SO_4^{2-} , mainly by heterogeneous conversion processes due to the absence of OH and thus little gas phase oxidation. This then scavenges gaseous NH_3 during night into NH_4HSO_4 and $(\text{NH}_4)_2\text{SO}_4$. There is a $\sim 50\%$ reduction in O_3 throughout the day related to the titration by high NO_x emissions. Looking at the diurnal changes in NO_x and NO_3^- shows that there is a rapid conversion of gaseous HNO_3 into particulate NO_3^- . The high deposition flux of HNO_3 (c.f. Table 2) results in a short tropospheric lifetime of hours, where thermal decomposition of particles transfers HNO_3 back into the gas phase, which explains the decrease in NO_3^- during the night i.e. a different equilibrium state is achieved. This is in spite of the potential for thermal decomposition of NH_4NO_3 being lower at night due to lower temperatures (c.f. Figure 9). Examining the diurnal profiles shows a similar behaviour occurs for NH_3 and NH_4^+ , whose evolution is coupled to NO_3^- in the ISORROPIA2 II parameterization. Both the NH_3 and NO_x emission remains relatively high across the simulation. The mixing ratios of HNO_3 , which are shown, are of the same order of magnitude as those measured during the BOP II measurement campaign undertaken at Cabauw.

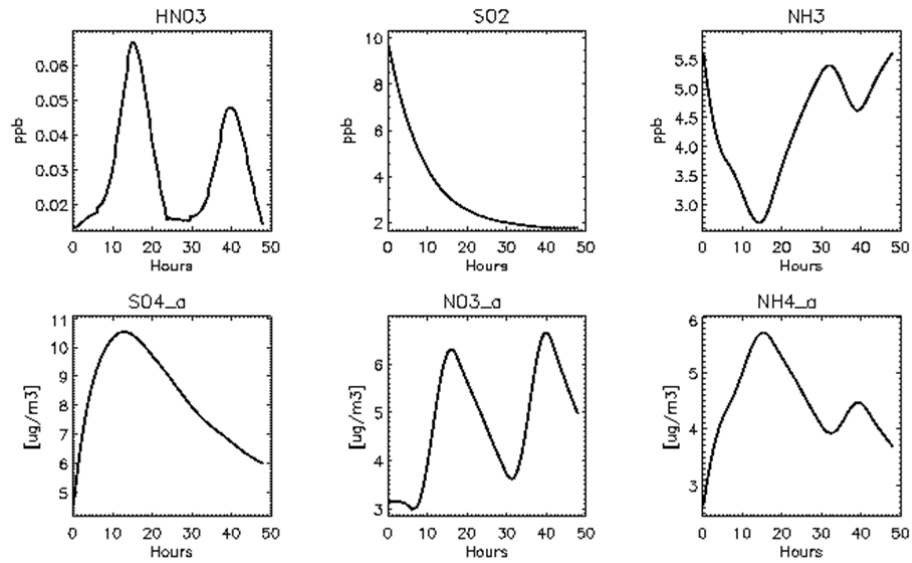


Figure 12: As for figure 10 except for an initial mixing ratio of 10 ppb ($26\mu\text{g}/\text{m}^3$) SO_2 .

Figure 12 shows the corresponding evolution of SIA for a more historical based scenario, where SO_2 concentrations are higher than those shown in Fig. 10. One main difference with the evolution of SIA in the historical scenario is that there is a continual increase in SO_4^- from the rather low initial condition for the first half of the first day, after which the loss rate begins to dominate the formation rate. This is due to a cumulative effect of lower $\text{SO}_{2(g)}$ in the second day, high deposition and the chemical conversion of SO_4^- into NH_4HSO_4 and $(\text{NH}_4)_2\text{SO}_4$. For NO_3^- , the profile closely follows that of HNO_3 , i.e. maximal concentrations occur around mid-day in line with the diurnal variation in OH (not shown). An associated decrease in NH_4^+ occurs, which represents a cumulative sum of the various forms of ammonium SIA as described by Eqns. (1), (3) and (4).

5. The daily variability in ammonium particle formation (K_{NH_3})

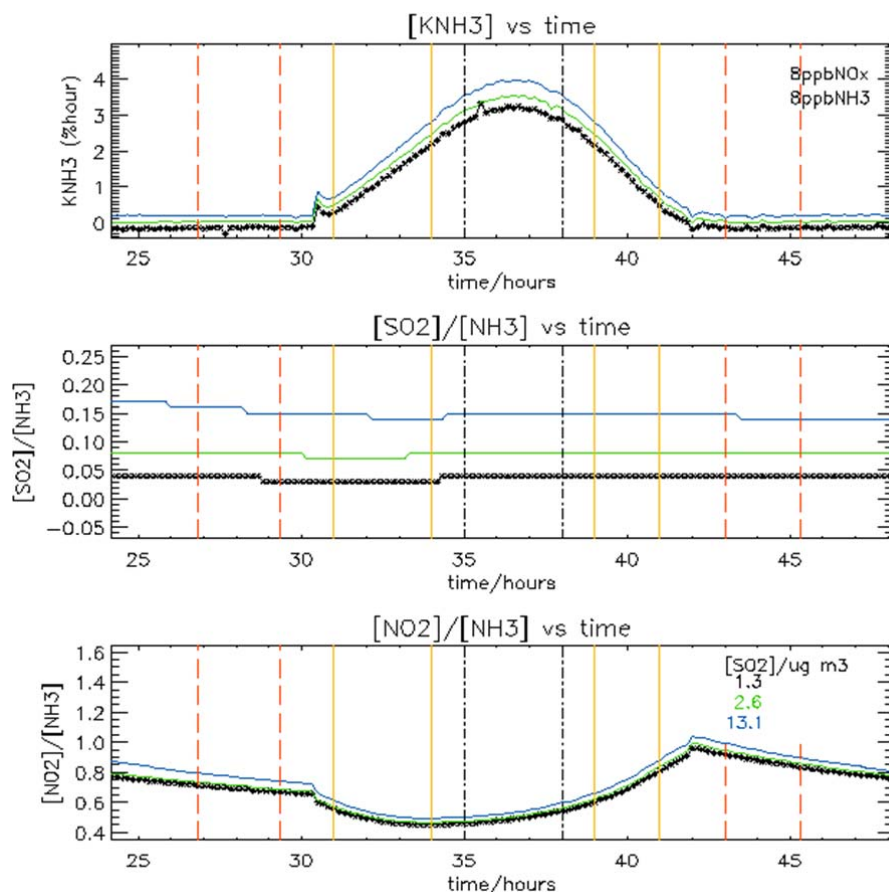


Figure 13: The daily variability in K_{NH_3} , C_1 and C_2 for a box-model simulation using 8 ppb ($9.8\mu\text{g}/\text{m}^3$) NO_x and 8 ppb ($5.5\mu\text{g}/\text{m}^3$) NH_3 . The initial SO_2 concentration for each of the three simulations is given in the inset. For each respective simulation with different SO_2 concentrations, the initial concentration and emissions of SO_2 are changed accordingly.

As the simulation progresses through the day the photochemical activity changes in line with the diurnal variability of solar irradiance. The subsequent variability in the OH radical imposes a diurnal cycle on the mixing ratio of HNO_3 (see top left panels in Figs. 11 and 12), which then subsequently changes the K_{NH_3} values (e.g. Danalatos and Glavas, 1999). Measurements in the field also observe a strong diurnal profile on particle number density (Takahama et al., 2004) related to the variability in chemical precursors, as shown in panels of Figs. 11 and 12. Figure 13 shows examples of how K_{NH_3} , C_1 and C_2 vary during the second day of a typical simulation. A large difference exists in both night-time and day-time values driven by the variability in the gaseous pre-cursors. The

highest rate of change of K_{NH_3} occurs during both the morning and early evening, which exhibit increasing and decreasing K_{NH_3} as time progresses, respectively. The vertical lines represent the sampling periods for night (red), morning/evening (yellow) and day (black).

5.1 Derivation of new ammonium particle formation rates

In order to derive a new parameterization for calculating K_{NH_3} we aggregate all of the C_1 , C_2 and K_{NH_3} values sampled during several hours across ~ 150 different box-model simulations and fit the resulting points to a surface using a second-order polynomial. Spurious points without associated changes to the C_1 and C_2 ratios are removed from the fitting procedure as they influence the final 'best-fit' parameters. A spurious point is defined as lying off the best-fit curve by more than 100%, where the number of points discarded is low compared to the total sample. Figures 14 and 15 show the resulting 'best' fit surfaces, along with the distribution of points around the surface for day (U1/U2 MSC) and night (S1/S2 MSC), respectively. The number of points used ranges from 8600 in the day and 7300 for the night. There is some scatter around the 'best-fit' surface, in part due to using variable meteorological parameters during the simulations (see Sect. 4.6). The resulting parameterizations derived from the day, morning/evening and night conversion values being described in Equations (6), (7) and (8) below:

$$k_{\text{NH}_3} (\text{U1/U2}) = 1.737 + 3.81C_1 + 8.675C_2 + 0.022C_1C_2 - 0.189C_1^2 - 0.194C_2^2 \quad (6)$$

$$k_{\text{NH}_3} (\text{N1/N2}) = 0.94 + 2.42C_1 + 7.281C_2 - 0.123C_1C_2 - 0.078C_1^2 + 0.248C_2^2 \quad (7)$$

$$k_{\text{NH}_3} (\text{S1/S2}) = -0.596 + 0.407C_1 + 0.597C_2 - 0.151C_1C_2 + 0.027C_1^2 + 1.10C_2^2 \quad (8)$$

The shape of each respective surface is quite different between the fits for the night and day conversion rates, being convex and concave, respectively. This results in lower K_{NH_3} values during night for corresponding C_1 and C_2 ratios. Diurnal variations in particle number density have been observed in field campaigns (Takahama et al., 2004) indicating that the diurnal variation in K_{NH_3} simulated in the box model is realistic and does occur in the troposphere.

Figure 16 provides a direct comparison of K_{NH_3} values derived using the morning/evening and day-time K_{NH_3} parameterizations, using the range of C_1 and C_2 ratios in the corresponding background maps for 2005 and 2015. There is a strong correlation which exists between the K_{NH_3} values until $K_{\text{NH}_3} > 30\%/hr$, after which some of the day K_{NH_3} values become lower than the corresponding morning/evening values.

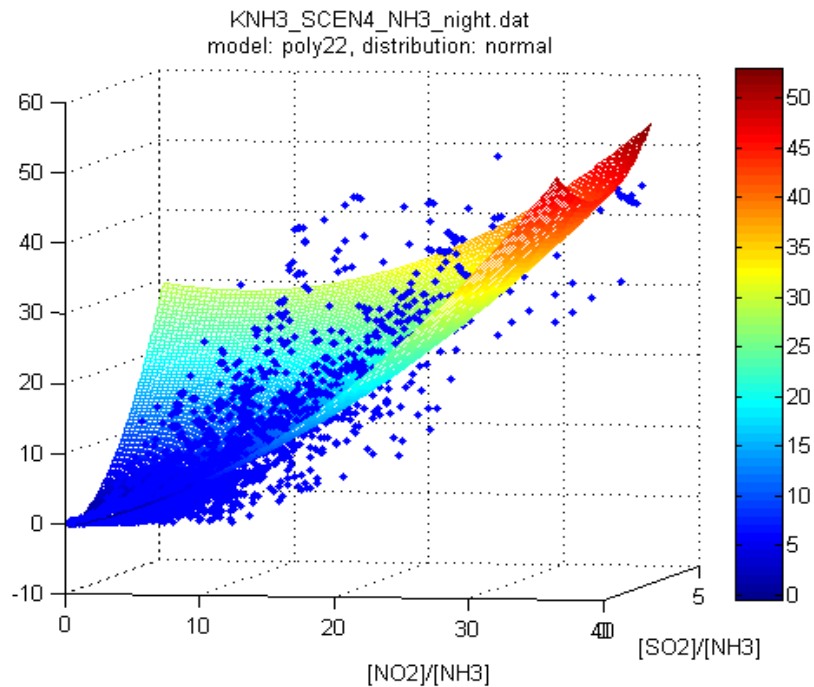


Figure 14: A second-order polynomial fit of K_{NH_3} values with C_1 ($[NO_2]/[NH_3]$) and C_2 ($[SO_2]/[NH_3]$) ratios for night-time conditions.

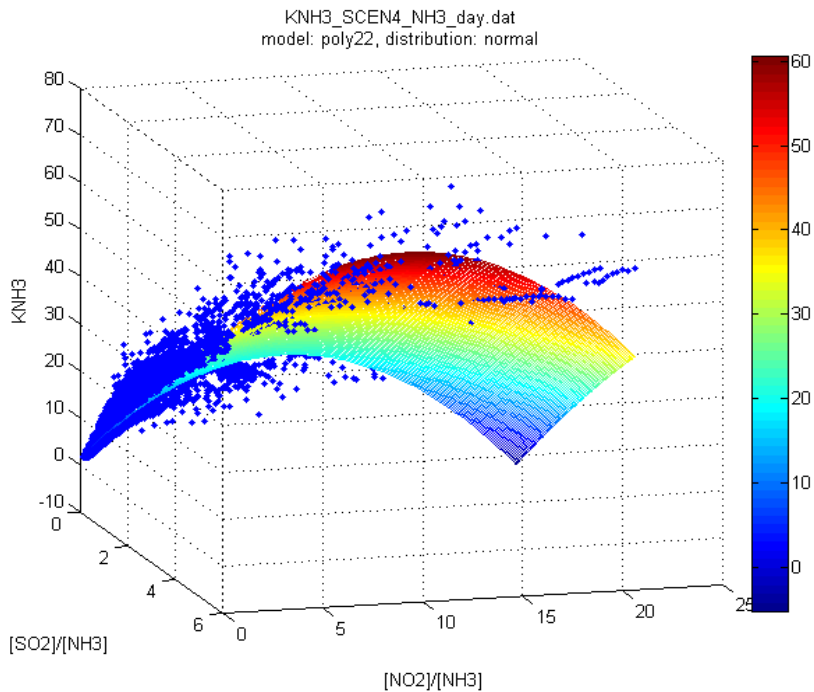


Figure 15: As for Figure 14 except for day-time conditions.

Figure 17 presents the corresponding correlation between K_{NH_3} values calculated using the day-time and night-time parameterizations, again linked with the background concentrations from the relevant maps. There is essentially low correlation between values, with the conversion of $NH_{3(g)}$ during the day being much faster than the

conversion which occurs during the night, especially for conversion rates which are $<20\% \text{ hr}^{-1}$. At higher K_{NH_3} values, the differences become less, although the number of incidences also decreases due to the relatively high C_1 and C_2 values.

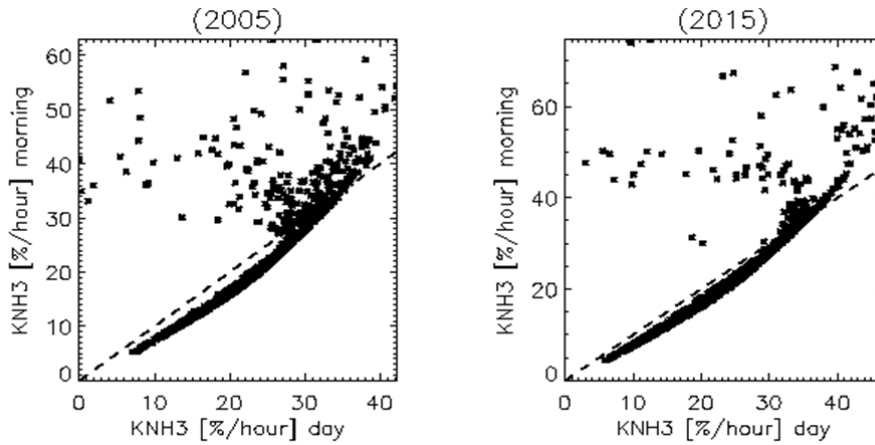


Figure 16: A comparison of K_{NH_3} values as calculated using morning/evening and day-time conditions for 2005 (left) and 2015 (right).

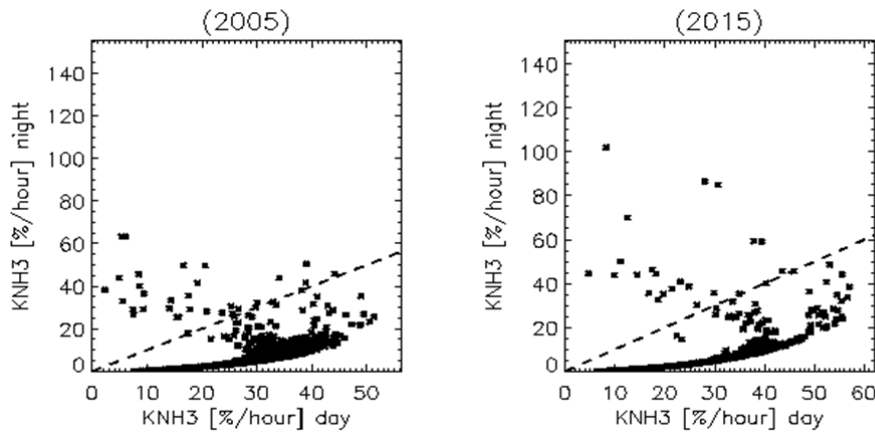


Figure 17: A comparison of K_{NH_3} values as calculated using night-time and day-time conditions for 2005 (left) and 2015 (right).

5.2 Sensitivity of K_{NH_3} towards meteorological parameters

In order to determine the effect of altering the meteorological parameters on the derivation of the parameterization (c.f. Fig. 10), a sensitivity test was performed where fixed values were adopted, namely temperature= 285°K , pressure= 1011.5 hPa and RH of 85%. Figures 18 and 19 show the correlation of the resulting K_{NH_3} values both with and without fixed meteorology for the night and day, respectively, along with the ideal correlation (dashed line). For the calculation of a valid range of K_{NH_3} , associated C_1 and C_2 values are taken from the background maps for 2005 and 2015.

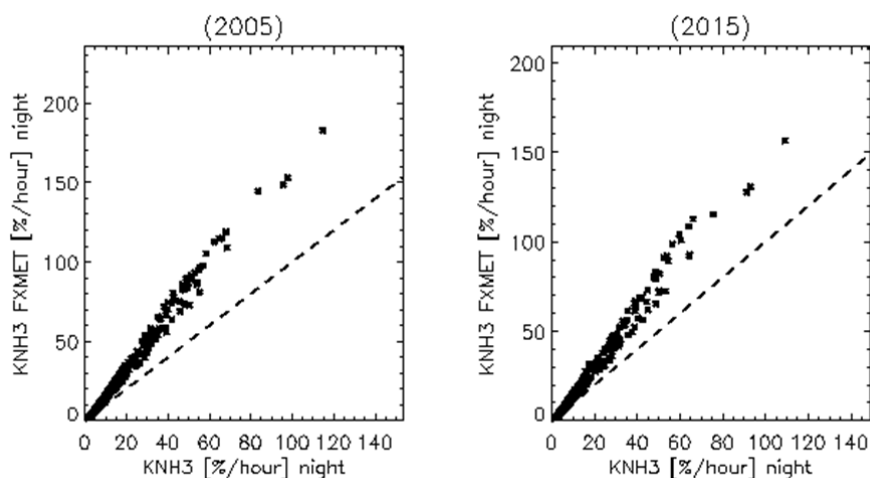


Figure 18: Correlation of K_{NH_3} values for night-time conditions between variable and fixed meteorology simulations.

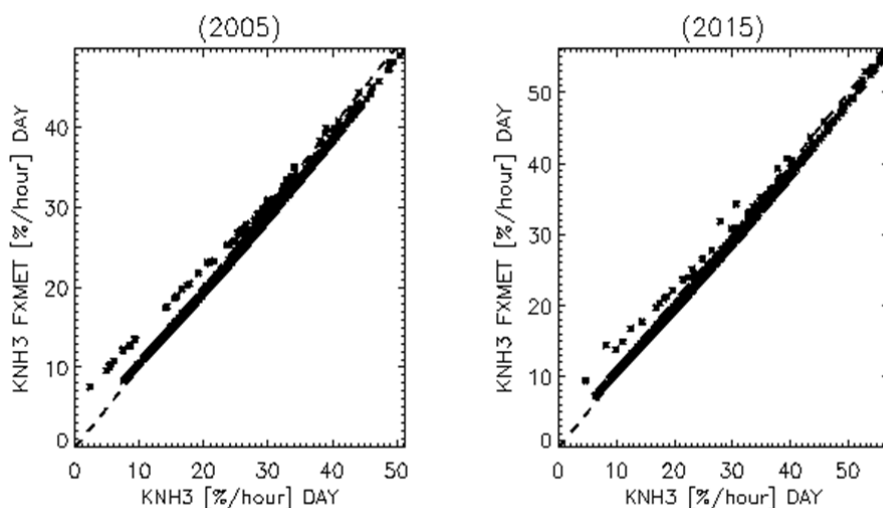


Figure 19: Correlation of K_{NH_3} values for day-time conditions between variable and fixed meteorology simulations.

Figure 18 shows that the sensitivity of K_{NH_3} towards the chosen meteorological parameters in the chemical 'box' model is rather large for night-time conditions. Conversely, for the day-time the K_{NH_3} parameterisation looks rather robust against meteorological variations. For both night and day the K_{NH_3} values are highly correlated, where fixing the meteorology results in higher K_{NH_3} values whenever the conversion rate is $> 15\% \text{ hr}^{-1}$. Moreover, the amount of variability (scatter) increases when changing the meteorology due to the sensitivity of NH_4^+ particle formation towards ambient temperatures. This sensitivity towards temperature agrees with field measurements, where NH_4^+ concentrations increase with respect to the altitude in the boundary layer, due to a decrease in the particle volatility (Neuman et al, 2003).

5.3 Sensitivity of K_{NH_3} the prescribed deposition velocities

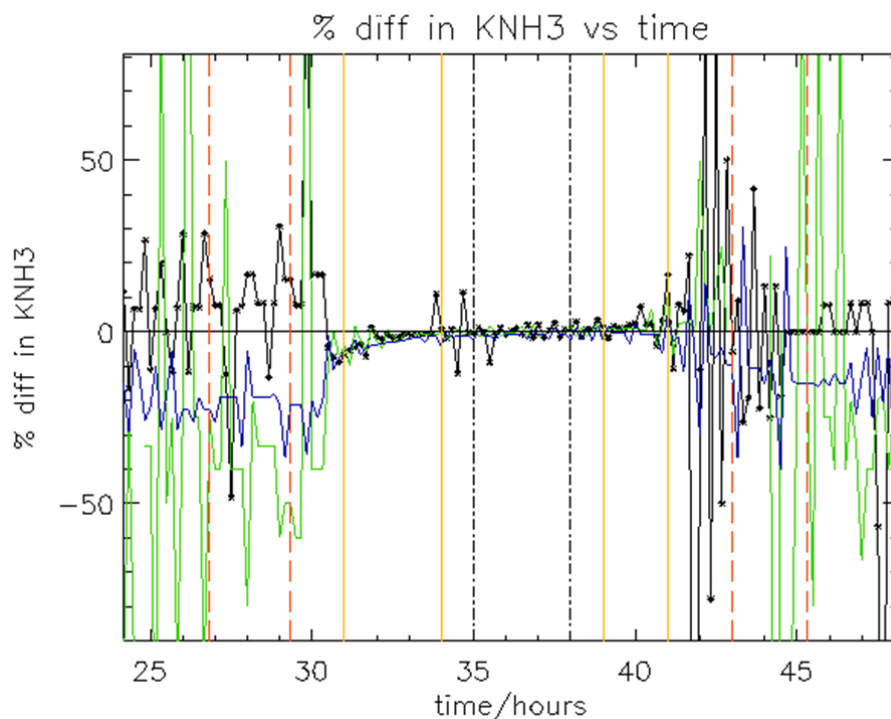


Figure 20: The percentage difference in K_{NH_3} values due to a 10% perturbation in the deposition fluxes applied in the chemical box model for the second simulation day. The percentage variability in K_{NH_3} values are shown for different SO_2 initial conditions, namely: 1.3 ug/m^3 SO_2 (black), 2.6 ug/m^3 (dark blue) and 13.1 ug/m^3 (neon green). The percentage difference is calculated as $(\text{SENS-BASE}/\text{SENS}) \cdot 100$.

To investigate the sensitivity of K_{NH_3} values on the deposition velocities, (i.e.) the integrated sink terms (venting, wet deposition, dry deposition) prescribed in the chemical box model, we perform a simulation where the deposition velocities for HNO_3 , NH_4^+ , SO_4^- and NO_3^- are decreased by 10%. We subsequently investigate the percentage difference introduced into the K_{NH_3} value with respect to time for the second day of the simulation, where sampling takes place for the derivation of the new parameterizations. The variability of deposition velocities with respect to land surface is typically larger than 10%, meaning that this acts as a rather conservative sensitivity test.

Figure 20 shows that percentage difference in the K_{NH_3} values with respect to simulation time, where the difference is calculated as $(\text{SENS-BASE}/\text{BASE}) \cdot 100$. The periods where sampling occurs for the night-time (red dashed), morning (yellow) and day-time (black, dot-dash) parameterizations are shown as the vertical transects. The morning/evening and day-time K_{NH_3} values are quite robust and exhibit a low sensitivity to the prescribed deposition flux in their respective sampling windows. The diurnal variability in the magnitude of K_{NH_3} means that small changes in the night-time K_{NH_3} values result in appreciable differences. Thus, such K_{NH_3} values are much more sensitive to the variability in the prescribed deposition velocity.

There is also a dependency on the prescribed SO_2 concentrations as shown by the different coloured lines. For morning/evening and day-time values, differences are typically under 10% across all conditions, whereas for night-time values the differences increase significantly to greater than 50% within the sampling period, especially for conditions of relatively high SO_2 concentrations. That the largest variability introduced into K_{NH_3} occurs around midnight, coinciding with times outside the sampling windows for the derivation of the NH_4^+ parameterization, means that the uncertainty introduced is limited somewhat. Thus, there is much more confidence in the day-time parameterization when compared with the corresponding night-time parameterization due to the respective sensitivities with respect to deposition velocities.

5.4 Sensitivity of K_{NH_3} towards prescribed boundary layer height

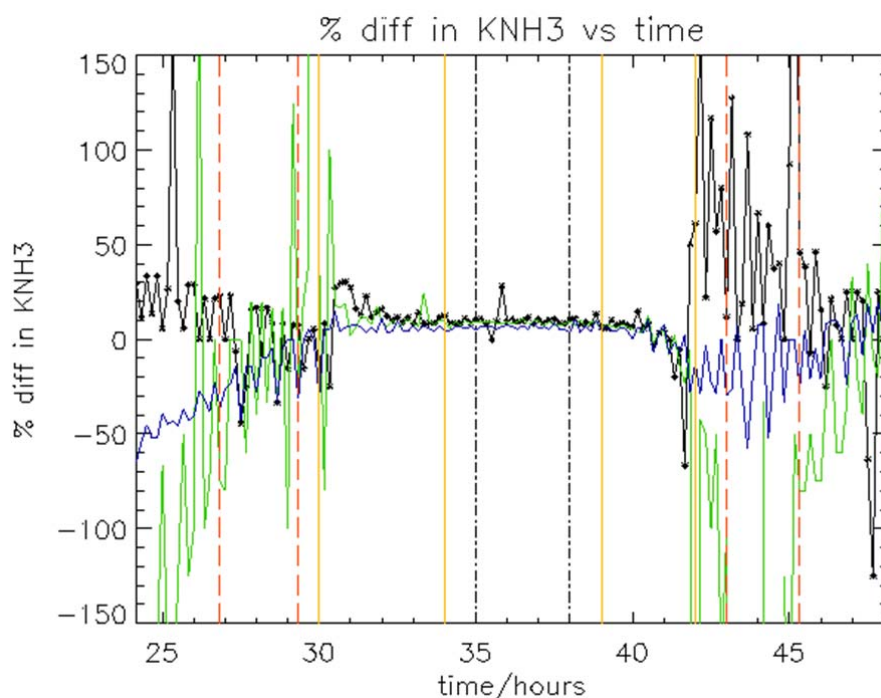


Figure 21: The corresponding percentage difference in K_{NH_3} values due to a 20% decrease in the boundary layer height to 400m.

To investigate the sensitivity of K_{NH_3} values on the prescribed boundary layer height we decrease it from the default setting of 500m to 400m, which is within the range of the values adopted across the MSC classes as given in Table 1. Observations have shown that the diurnal evolution of the boundary layer plays a critical role in determining SIA particle concentrations in the boundary layer (Väkevä et al., 2000). Similar to the sensitivity towards prescribed deposition velocities discussed above, the day-time K_{NH_3} are least sensitive to the prescribed boundary layer height, whereas the variability in the night-time values is typically $\pm 100\%$. There is some implicit link in that the deposition values used are scaled by the surface area of the cubic box, which is equal to the boundary layer height. No modifications are made to the emission fluxes that are employed, meaning that the box becomes slightly more polluted when it is reduced in size as the same mass is added per chemical time step. The magnitude of the variability is larger than that calculated for the sensitivity test discussed in Sect. 5.3.

6. Comparisons of particle formation rates

6.1 Spatial distribution of K_{NH_3} values for sample years

In this section we discuss the differences in the spatial variability in K_{NH_3} values for the Netherlands resulting from the various parameterizations discussed in Sect. 3 and 4.5. Figure 22 shows the spatial distribution of K_{NH_3} values for both 2005 and 2015 calculated using the old parameterization (c.f. Eqn. 5) by adopting the C_1 and C_2 values shown in Figs. 4 and 5. It is interesting to see that a fraction of the domain is white around Rotterdam, indicating negative values occur for K_{NH_3} whenever the C_2 ratio exceeds a certain threshold. These white grid cells correspond with a default conversion rate of 1%. However, in OPS this 1% K_{NH_3} rate is never actually used, as whenever the C_2 ratio exceeds 3.0, the K_{NH_3} value is set equal to that calculated for a C_2 ratio of 3.0 i.e. an upper limit is imposed resulting in K_{NH_3} values $> 100\%/hr$ for such grid cells (c.f. Fig. 3).

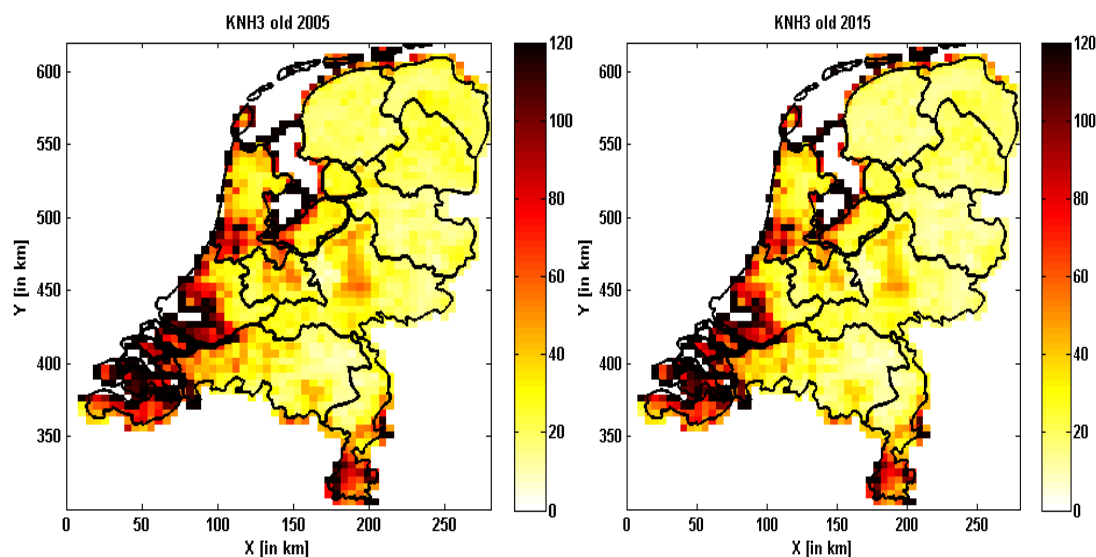


Figure 22: The spatial distribution of K_{NH_3} values for 2005 (left) and 2015 (right) on a 5 x 5 km resolution calculated using the Eqn (5) using C_1 and C_2 input values taken from the corresponding background maps

A comparison of the spatial distribution in K_{NH_3} for 2005 and 2015 shows that a similar spatial pattern is evident between the present (2005) and future (2015) years. Decreases in K_{NH_3} values can be seen around sensitive areas e.g. Gelderland mainly due to the mitigation of NO_x emissions from the transport sector. Although the distribution shown in Fig. 22 is relevant for the individual grid points, OPS uses C_1 and C_2 ratios which are the average of 20 sampled points between any source and receptor point. Thus, lower effective C_1 and C_2 ratios are applied in OPS, rather than the extreme K_{NH_3}

values shown around the coast and industrial centres. Moreover, the background concentrations of both SO_2 and NO_2 are also corrected for the relevant wind direction using measurements taken in 2003, further complicating the derivation of the C_1 and C_2 ratios.

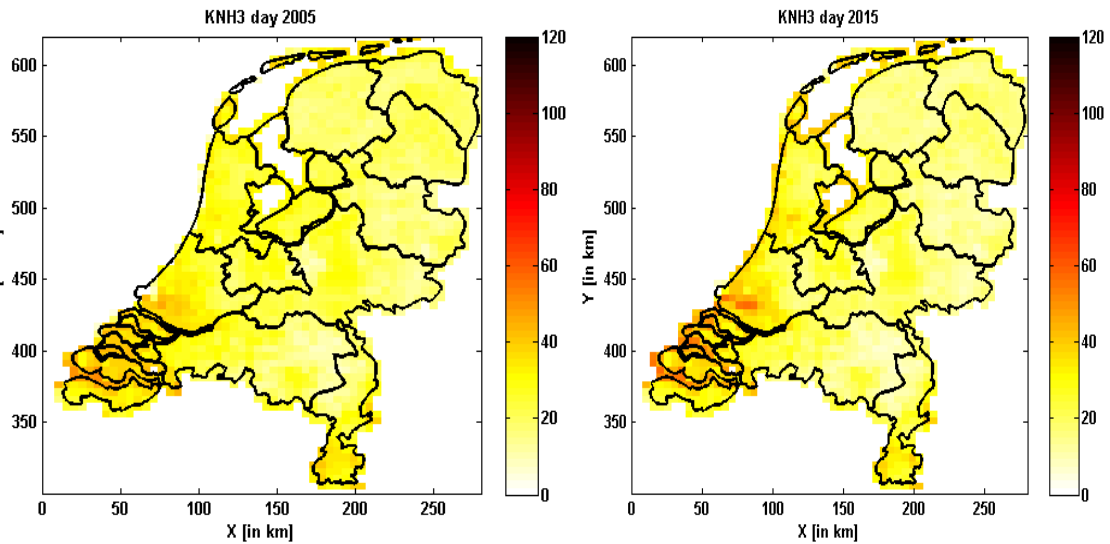


Figure 23: As for Fig. 22 except using Eqn. (6) (day-time conversion rates) to calculate the temporal distribution of K_{NH_3} values.

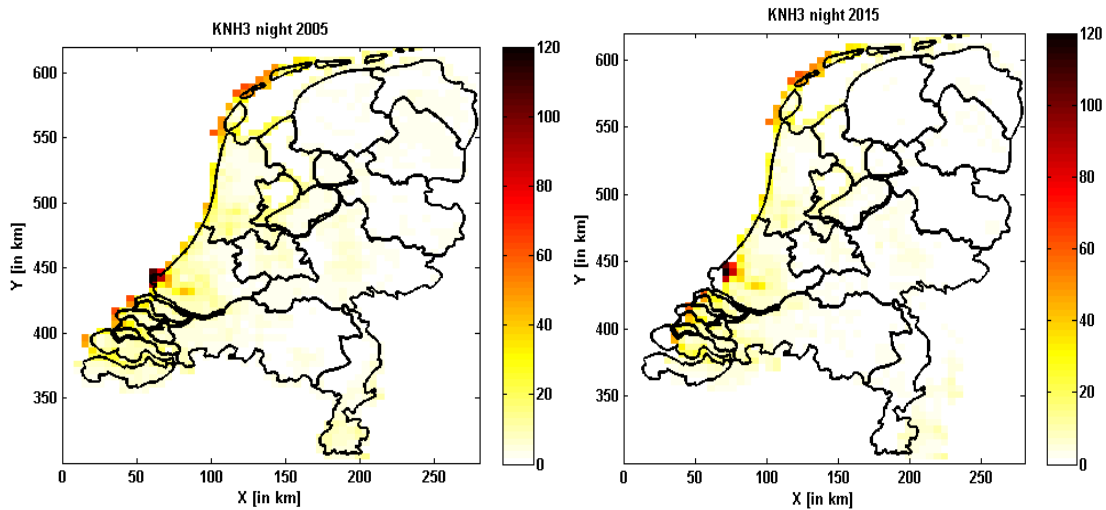


Figure 24: As for Fig. 23 except using Eqn. (8) (night-time conversion rates) to calculate the temporal distribution of K_{NH_3} values.

Figures 23 and 24 show the corresponding spatial distributions in K_{NH_3} using the day-time and night-time parameterizations in the form of Eqns. 6 and 7, respectively. The highest K_{NH_3} values are ~ 50 when using the day-time parameterization, which is $\sim 50\%$ lower than the highest K_{NH_3} values shown in Fig. 22. Thus, applying these new parameterizations in the OPS will likely reduce the rate of particle formation. For the

night-time parameterization, the differences are even larger, with K_{NH_3} values being significantly lower than the corresponding day-time conversion rates.

6.2 The application of new K_{NH_3} values in the OPS model

To assess whether the new parameterization improves the performance of the OPS model compared to measured values, we have performed test simulations where Eqn (6) is applied across all MSC and subsequently compared it with both the original parameterization and the integrated effect of using Eqns (6)-(8). Each respective formation rate (night-time (S class), morning/evening (N class) and day-time (U class)) is indexed online in the OPS using the MSC for a number of sequential trial years (2009-2012).

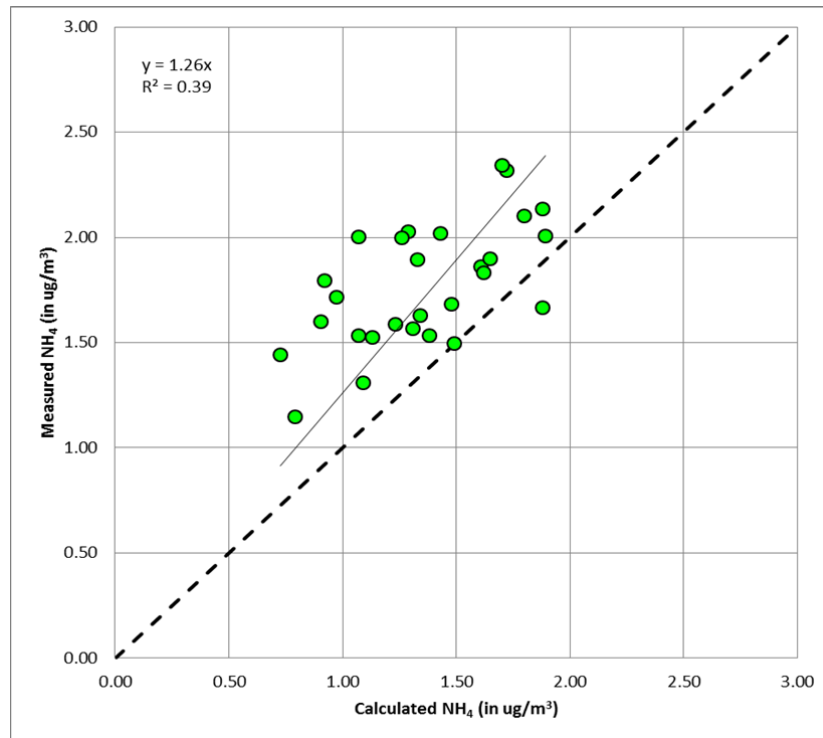


Figure 25: The correlation of the annually averaged NH_4^+ concentrations measured at 7 different stations across the Netherlands between 2009-2012 with that modelled in OPS using the original parameterization for particle formation described in Equation (5).

Figures 25-27 show the resulting correlation between measured and modelled annual totals for the seven measurement sites shown in Fig. 2, respectively. When comparing the various figures, it can be seen that when averaged between 2009 and 2012, the slope of the regression when applying Eqn (6) across all MSC is ~ 1.14 , which improves on the original parameterization, which has corresponding value of ~ 1.26 .

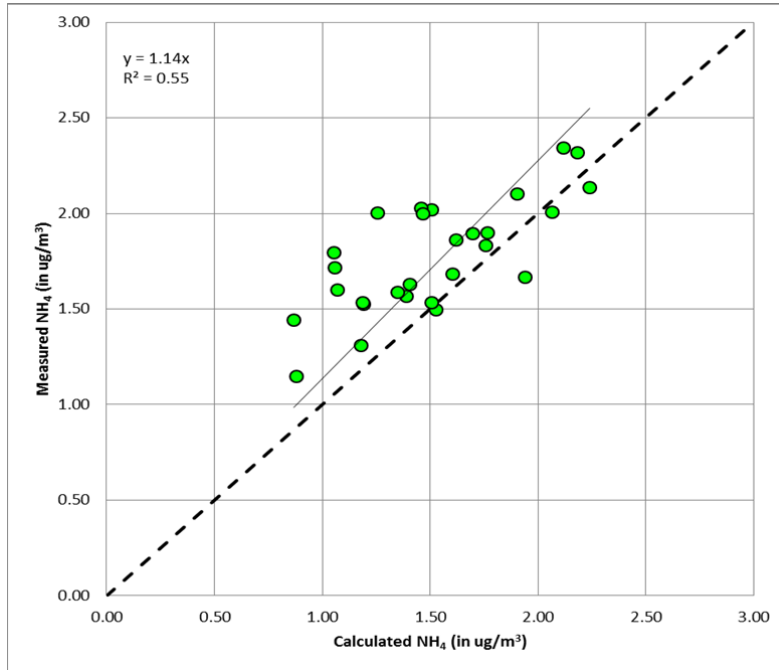


Figure 26: The correlation of the annual averaged NH_4^+ concentration as measured at 7 different stations across the Netherlands between 2009-2012 with that modelled in OPS using Eqn (6).

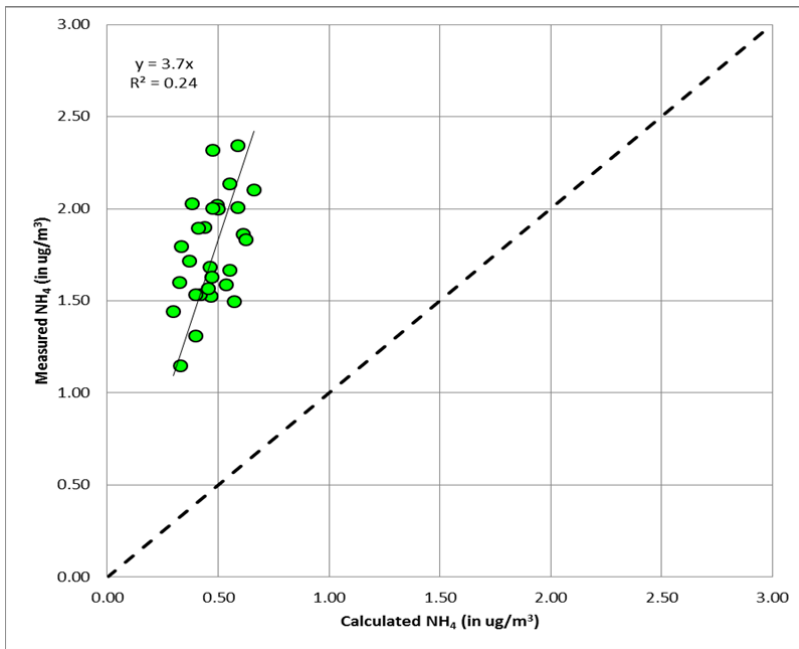


Figure 27: The correlation of the annual averaged concentration of ammonium measured at 7 different stations across the Netherlands between 2009-2012 with that modelled in OPS using Eqns (6), (7) and (8) indexed using the various MSC.

7. Summary

In this report we have presented the methodology, derivation and application of a new parameterization for calculating ammonium (NH_4^+) particle formation for use in the Operational Priority Substances (OPS) model. The new parameterization calculates the hourly conversion rate of gaseous ammonia (K_{NH_3}) into NH_4^+ as a function of the concentration ratios of sulphur dioxide, ammonia and nitrogen dioxide using the output from a chemical 'box' model that includes the ISORROPIA II module for calculating the conversion of gaseous pre-cursors into secondary inorganic aerosol. The stability of the resulting SIA is dependent on both temperature and relative humidity, where we apply values taken from the meteorological classes defined in the OPS.

By sampling K_{NH_3} throughout the day, we show that there is a large difference in the magnitude of K_{NH_3} calculated for night-time, morning/evening and day-time conditions due to the diurnal variation in nitric acid, an important pre-cursor for particle formation. A strong diurnal variation in SIA formation is reported in the literature based on a number of independent observations. In that the sampling frequency of the six different meteorological classes in the OPS exhibit some type of diurnal dependency means that, theoretically, different parameterizations may be used with respect to the time of the day. Using the temporal distribution and variability of $[\text{SO}_2]/[\text{NH}_3]$ and $[\text{NO}_2]/[\text{NH}_3]$ throughout the Netherlands, as defined in background maps used within the OPS model, we show that the new parameterization is able to provide conversion rates across a wide range of conditions.

We have tested the robustness of the 'best-fit' parameterizations with respect to meteorological conditions (temperature, relative humidity and surface pressure), boundary layer height and deposition velocities. We find that the day-time and morning K_{NH_3} values are relative robust exhibiting a maximum variability of around 10%. However, the night-time values are sensitive to the prescribed conditions, due to the rather low K_{NH_3} values.

Applying the various parameterizations online in the OPS shows that when applying the three independently derived K_{NH_3} parameterizations, a significant decrease in the slope of the regression occurs i.e. OPS significantly under predicts the annually averaged concentration of NH_4^+ measured at the seven measurement sites throughout the Netherlands. However, only applying the day-time parameterization in OPS does result in an improvement in the performance of OPS, leading to an overall regression slope of 1.14 and an r^2 value of 0.55. Further tests in OPS are needed, where indexing of different formation rates with respect to distance classes should be tested in more detail.

8. References

- Aan de Brugh, J. M. J., J. S. Henzing, M. Schaap, W. T. Morgan, C. C. van Heerwaarden, E. P. Weijers, H. Coe and M. C. Krol (2012) Modelling the partitioning of ammonium nitrate in the convective boundary layer, *Atmos. Chem. Phys.*, 12, 3005-3023.
- Bouwman, A. F., D. S. Lee, W. A. H. Asman, F. J. Dentener, K. W. van der Hoek and J. G. J. Olivier (1997) A global high-resolution emission inventory for ammonia, *Global, Bio. Chem. Cy.*, 11, 561-587.
- Danalatos, D. and Glavas, S. (1999) Gas phase nitric acid, ammonia and related particle matter at a Mediterranean coastal site, Patras, Greece, *Atms. Environ.*, 33, 3417-3425.
- de Leeuw, F. A. A. M., H. J. van Rheineck-Leyssius and P. J. H. Buitjes (1990). Calculation of the long term averaged ground level ozone concentrations, *Atmospheric Environment*, 24A, 185-193.
- Ervens, B., George, C., Williams, J. E., Buxton, G. V., Salmon, G. A., Bydder, M., Wilkinson, F., Dentener, F., Mirabel, P., Wolke, R., and Herrmann, H. (2003) CAPRAM 2.4 (MODAC mechanism): An extended and condensed tropospheric aqueous phase mechanism and its application, *J. Geophys. Res.*, 108 (D14), 4426-4447.
- Fountoukis, C. and A. Nenes (2007). ISORROPIA II: a computationally efficient thermodynamic equilibrium model for K^+ - Ca^{2+} - Mg^{2+} - NH_4^+ - SO_4^{2-} - NO_3^- - Cl - H_2O aerosols, *Atms. Phys. Chem.*, 7, 4639-4659.
- Geels, C., H. V. Anderson, C. A. Skjøth, J. H. Christensen, T. Ellermann, P. Løfstrøm, S. Gyldenkaerne, J. Brandt, K. M. Hansen, L. M. Frohn and O. Hertel (2012) Improved modeling of atmospheric ammonia over Denmark using the coupled modeling system DAMOS, *Biogeosciences*, 9, 2625-2647.
- Geleyn, J. F. and A. Hollingsworth (1979) An Economical analytical method for the computation of the interaction between scattering and line absorption of radiation, *Contrib. Atms. Phys.*, 51 (1), 1-16.
- Guenther, A. B., Jiang, X., Heald, C. L., Sakulyanontvittaya, T., Duhl, T., Emmons, L. K. and Wang, X. (2012) The Model of Emissions of Gases and Aerosols from Nature version 2.1 (MEGAN2.1): an extended and updated framework for modeling biogenic emissions, *Geosci. Model Dev.*, 5, 1471-1492.
- Van Jaarsveld, H., Sauter, F., van Zanten, M., van der Swaluw, E., Aben, J. and de Leeuw, F. (2012) The OPS-model: Description of OPS 4.3.15, RIVM technical report.
- Neuman, J. A., Nowak, J. B., Brock, C. A., Trainer, M., Fehsenfeld, F. C., Holloway, J. S., Hübler, G., Hudson, P. K., Murphy, D. M., Nicks Jr, D. K., Orsini, D., Parrish, D. D., Ryerson, T. B., Sueper, D. T., Sullivan, A. and Weber, R. (2003) Variability in ammonium nitrate formation and nitric acid depletion with altitude and location over California, *J. Geophys. Res.*, 108(D17), 4557.

NOAA (1976) US Standard Atmosphere, National Oceanic and Atmospheric Administration NOAA-S/T76-1562, Washington D. C., U. S. Gov. Printing office, 227.

Pinder, R. W., R. Strader, C. I. Davidson, and P. J. Adams (2004) A temporally and spatially resolved ammonia emission inventory for dairy cows in the United States, *Atmos. Environ.*, 38, 3747-3756.

Sander, S. P., J. R. Abbatt, J. B. Burkholder, R. R. Friedl, D. M. Golden, R. E. Huie, C. E. Kolb, G. Kurylo, K. Moortgat, V. L. Orkin and P. H. Wine (2011) Chemical kinetics and Photochemical Data for Use in Atmospheric studies, Evaluation No.17, JPL Publication 10-6, Jet Propulsion Laboratory, Pasadena, available at: <http://jpldataeval.jpl.nasa.gov>, 2011.

Seinfeld, J. H. and S. N. Pandis (2006) *Atmospheric chemistry and Physics: From Air Pollution to Climate Change*, John Wiley & Sons Inc. New York, 1-1203.

Shettle, E. P. and R. W. Fenn (1979) Models for the aerosols of the lower atmosphere and the effects of the humidity variations on their optical properties, *Environ. Res. Paper*, 676, AFGL-TR-79-0114, 91pp, 1979.

Skjøth, C. A. and C. Geels (2013) The effect of climate and climate change on ammonia emissions in Europe, *Atms. Chem. Phys.*, 13, 177-128.

Slingo, A. (1989) A GCM parameterization for the shortwave radiative properties of water clouds, *J. Atmos. Sci.*, 46, 1419-1427.

Stevens, C. J., C. Dupre, E. Dorland, C. Gaudnik, D. J. G. Gowling, A. Bleeker, M. Diekmann, D. Alard, R. Bobbink, D. Fowler, E. Corcket, J. O. Mountford, V. Vandvik, P. A. Aarrestad, S. Müller and N. B. Dise (2010) Nitrogen deposition threatens species richness of grasslands across Europe, *Environ. Pollut.*, 158, 2940-2945.

Sutton, M. A., O. Oenema, J. W. Erisman, A. Leip, H. van Grinsven and W. Winiwarter (2011) Too much of a good thing, *Nature*, 472, 159-161.

van der Swaluw, E., Denier van der Gon, H., Hendriks, C., Hoogerbrugge, R., Matthijsen, J., Keuken, M., Schaap, M., Weijers, E., Wichink Kruit, R. (2013) Summary of the second Netherlands Research Program on Particulate Matter (BOP II). RIVM Report 680356002

Takahama, S., Wittig, A. E., Vayenas, D. V., Davidson, C. I. and Pandis, S. N. (2004) Modeling the diurnal variation of nitrate during the Pittsburgh Air Quality Study, *J. Geophys. Res.*, 109, D16S06.

Tang, I. N., W. T. Wong and H. R. Munkelwitz (1967) The relative importance of atmospheric sulfates and nitrates in visibility reduction, *Atms. Environ.*, 15(12), 2463-2471.

van der Werf, G. R., Randerson, J. T., Giglio, L., Collatz, G. J., Mu, M., Kasibhatla, P. S., Morton, D. C., DeFries, R. S., Jin, Y. and van Leeuwen, T. T (2010) Global fire emissions and the contribution of deforestation, savanna, forest, agricultural, and peat fires (1997–2009), *Atms. Chem. Phys.*, 10, 11707-11735.

Väkevä, M., Hämaeri, H., Puhakka, T., Nilsson, E. D., Hohti, H. and Mäkelä, J. M. (2000) Effects of meteorological processes on aerosol particle distribution in an urban background area, *J. Geophys. Res.*, 105(D8), 9807-9821.

Velders G.J.M., J.M.M. Aben, B.A. Jimmink, G.P. Geilenkirchen, E.van der Swaluw, W.J. de Vries, J. Wesseling and M.C. van Zanten (2013) Grootschalige concentratie-en depositiekaarten Nederland Rapportage 2012. RIVM Report 680362002

Verwer, J. G. (1994) Gauss-Seidel iteration for stiff ODEs from chemical kinetics, *SIAM J. Sci. Comput.*, 15, 1243-1250.

Weijers E.P., G.P.A. Kos, M.J. Blom, R.P. Otjes, M. Schaap and E. van der Swaluw (2012). Measurements of secondary inorganic aerosols in the Netherlands, ECN report. ECN-E-12-003

Wichink Kruit R.J., M. Schaap, F.J. Sauter, E. van der Swaluw and E.Weijers (2012). Improving the understanding of the secondary inorganic aerosol distribution over the Netherlands, TNO report. TNO-060-UT-2012-00334

Williams, J. E., J. Landgraf, A. Bregman, and H. Walter (2006). A modified band approach for the accurate calculation of online photolysis rates in stratospheric-tropospheric Chemical Transport Models, *Atmos. Chem. Phys.*, 6, 4137-4161, doi:10.5194/acp-6-4137-2006.

Williams, J. E. and T. P. C. van Noije (2008). On the upgrading of the modified Carbon Bond Mechanism for use in global Chemistry Transport Models, WR 2008-02, KNMI, De Bilt.

Williams, J. E., A. Strunk, V. Huijnen and M van Weele (2012). The application of the Modified Band Approach for the calculation of on-line photodissociation rates in TM5: implications for oxidative capacity, *Geosci. Model. Dev.*, 5, 15-35.

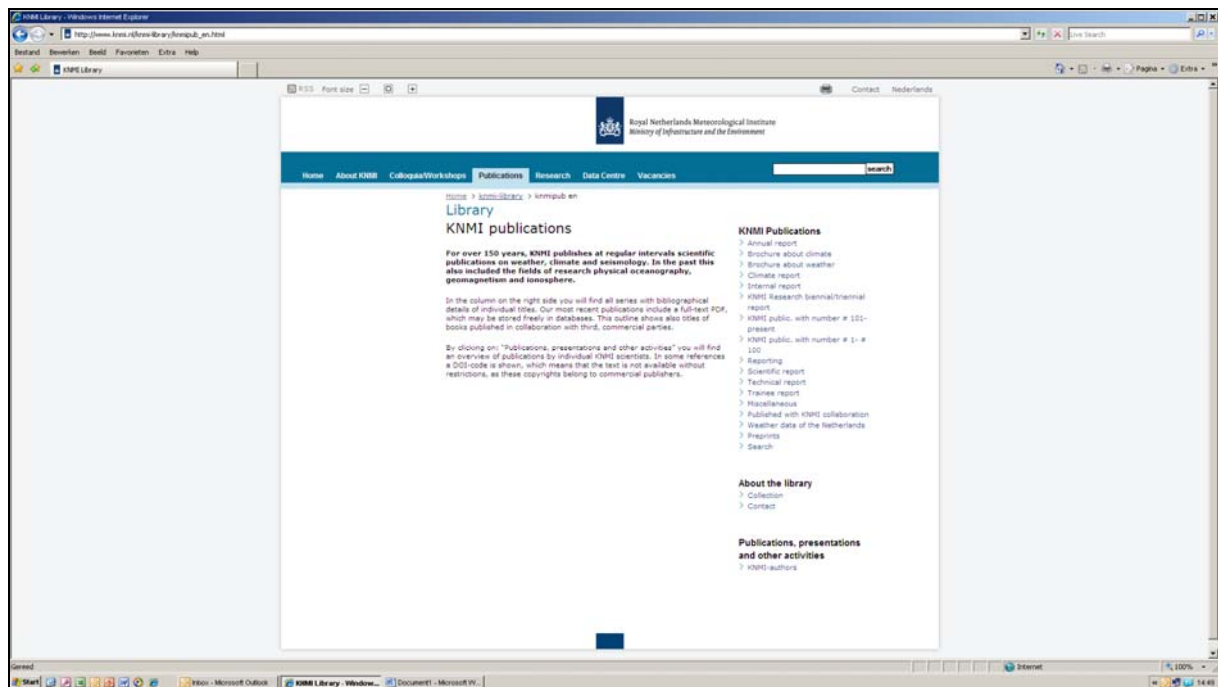
Yarwood, G., S. Rao, M. Yocke and G. Whitten (2005). Updates to the carbon bond mechanism: CB05. Final report to the US EPA, EPA Report Number: RT-0400675, available at: www.camx.com.

Xu, L. and J. E. Penner (2012) Global simulations of nitrate and ammonium aerosols and their radiative effects, *Atms. Chem. Phys.*, 12, 9479-9504.

Zdunkowski, W. G., R. M. Welsch, and G. J. Korb (1980): An investigation of the structure of typical 2-stream methods for the calculation of solar fluxes and heating rates in clouds, *Contrib. Atmos. Phys.*, 53, 215-238.

A complete list of all KNMI -publications (1854 – present) can be found on our website

www.knmi.nl/knmi-library/knmipub_en.html



The most recent reports are available as a PDF on this site.

